



Pr:Ca_{1-x}R_xF_{2+x} (R=Y or Gd) crystals: Modulated blue, orange and red emission spectra with the proportion of R³⁺ ions

Hao Yu ^{a,d}, Xiaobo Qian ^a, Linyang Guo ^b, Dapeng Jiang ^a, Qinghui Wu ^a, Fei Tang ^a,
Liangbi Su ^{a,e,*}, Qiangwen Ju ^a, Jingya Wang ^a, Jun Xu ^{c,**}

^a Synthetic Single Crystal Research Center, CAS Key Laboratory of Transparent and Opto-functional Inorganic Materials, Shanghai Institute of Ceramics, Chinese Academy of Sciences, No. 588 Heshuo Road, Shanghai 201899, China

^b State Key Laboratory on High Power Semiconductor Lasers, Changchun University of Science and Technology, No. 7989 Weixing Road, Changchun 130022, Jilin, China

^c School of Physics Science and Engineering, Institute for Advanced Study, Tongji University, Shanghai 200092, China

^d University of Chinese Academy of Sciences, No. 19A Yuquan Road, Beijing, 100049, China

^e State Key Laboratory of High Performance Ceramics and Superfine Microstructure, Shanghai Institute of Ceramics Chinese Academy of Sciences, Shanghai, 20050, China



ARTICLE INFO

Article history:

Received 13 June 2017

Received in revised form

12 December 2017

Accepted 8 February 2018

Available online 14 February 2018

Keywords:

Pr:Y(Gd):CaF₂ single crystals
Modulated spectral properties
Visible luminescence

ABSTRACT

The spectroscopic properties of 0.6at.‰:Pr:Ca_{1-x}R_xF_{2+x} (R = Y, Gd; x = 0.006, 0.012, 0.03, 0.06) crystals were investigated and compared. The XRD tests were conducted and the cell dimensions of the crystals were calculated. Room temperature absorption spectra have been registered and analyzed. The emission spectra and decay curves of the crystals were obtained at room temperature. Increasing the proportion of the lattice regulators of Y³⁺ or Gd³⁺ ions could significantly enhance the luminescence intensity of all visible emission bands with different ratios. Particularly, the emission intensity ratio of orange to red increased from 0.15 to 1.9 in Pr:Ca_{1-x}Y_xF_{2+x} crystals and to 1.02 in Pr:Ca_{1-x}Gd_xF_{2+x} crystals, respectively. Furthermore, Pr:Ca_{1-x}Gd_xF_{2+x} crystals have substantially strong emission at orange and red region of 580–660 nm, comparable with blue light at 482 nm. The quantum efficiency of the crystals increased rapidly with the increment of R³⁺ concentration, and finally tend to be 100%.

© 2018 Elsevier B.V. All rights reserved.

1. Introduction

In the last two decades, materials doped with trivalent praseodymium Pr³⁺ ions have been receiving considerable interest for emitting solid state lasers in the visible spectral range, which are applied to laser display technology, medical laser therapy equipment and laser distance measurement. The rich Pr³⁺ energy level can offer a large range of laser transitions in the blue, green, orange, red, and deep red spectral regions. The Pr-laser was first realized using Pr:YLF in the blue region by using a pulsed dye laser in 1977 [1]. While the efficiency was quite low because of the

insufficient overlapping between the pump wavelength and the absorption peaks of the Pr³⁺ ions doped crystals, hence the search of host materials for praseodymium has become a research hotspot in the recent years [2–8]. The development of the pumping sources has promoted the research process of the Pr³⁺ ions doped crystals in the field of laser. The GaN/InGaN laser diodes provide a 445 nm blue light, which corresponds with ³H₄→³P₂ absorption peak of Pr³⁺ ions. Several visible laser operations pumped by the GaN laser diodes have been realized in recent years in both oxide crystals and fluoride crystals, such as YAlO₃ [9], SrAl₁₂O₁₉ [10], LiYF₄ [11–14], KY₃F₁₀ [15], BaY₂F₈ [16], LiLuF₄ [17]. Compared with oxide crystals, the fluoride crystals have a lower phonon energy, which is beneficial to generating highly efficient lasers. Among several fluorides crystal hosts, calcium fluoride crystal (CaF₂) is a promising laser host because of its excellent optical and physical characteristics, such as broad transmission range (0.125–10 μm) [18], low phonon energy and good thermal conductivity (9.71 W/m·K for the pure CaF₂ crystal) [19–21].

* Corresponding author. Synthetic Single Crystal Research Center, CAS Key Laboratory of Transparent and Opto-functional Inorganic Materials, Shanghai Institute of Ceramics, Chinese Academy of Sciences, No. 588 Heshuo Road, Shanghai 201899, China.

** Corresponding author.

E-mail addresses: suliangbi@mail.sic.ac.cn (L. Su), xujun@mail.schnc.ac.cn (J. Xu).

Rare-earth ion doped CaF_2 have already achieved many breakthroughs during last years. An diode-pumped chirped-pulse amplifier (CPA) laser system, POLARIS in Germany, with a terawatt output power [22], has been demonstrated by using $\text{Yb}:\text{CaF}_2$ single crystals as the amplifying medium in 2008. An amplified chirped laser with pulse energy of 54.2 J has also been achieved with the aid of $\text{Yb}:\text{CaF}_2$ as the active medium in 2016 [23]. Furthermore, in $\text{Nd}:\text{Y}:\text{CaF}_2$ crystal, Qin et al. [24] achieved an ultra-short pulse laser of 103 fs using passive mode-locking technique. These outstanding results prove that CaF_2 crystal is an excellent laser host for the development of short-pulse and high-power diode-pumped solid-state lasers. Brian. M. et al. [25] have observed that Co-doping with Gd^{3+} or Y^{3+} had very drastic effects on both the cluster sites and relative intensities of lines in the emission spectra of the CaF_2 crystals. Serrano et al. [6] have researched on the spectral properties of Pr, R (R = Yb, Lu) crystals compared with the Pr singly doped CaF_2 crystal. An increase of the Pr^{3+} luminescence is observed in 0.5%Pr,10% Lu: CaF_2 crystal. J.L. Doualan et al. [26] have researched the effect of Y^{3+} ions on the emission spectrum of Pr: CaF_2 crystals. The energy transfer among the Pr^{3+} ions has been reduced and the $^3\text{P}_0$ emission quantum efficiency has been enhanced. While the specific effect of the concentration of regulating ions (Y^{3+} or Gd^{3+} ions) on the spectroscopic properties of the Pr: CaF_2 crystal has not been studied in detail. In this paper, we reported the spectroscopic properties 0.6at.%Pr: $\text{Ca}_{1-x}\text{Y}_x\text{F}_{2+x}$ and 0.6at.%Pr: $\text{Ca}_{1-x}\text{Gd}_x\text{F}_{2+x}$ crystals. The effects of the yttrium and gadolinium ions on the blue, orange and red emission behaviors in the Pr: CaF_2 crystals were discussed.

2. Material and methods

In our experiments, the 0.6at.%Pr-doped CaF_2 , $\text{Ca}_{1-x}\text{Y}_x\text{F}_{2+x}$ and 0.6at.%Pr: $\text{Ca}_{1-x}\text{Gd}_x\text{F}_{2+x}$ ($x = 0, 0.006, 0.012, 0.03, 0.06$) crystals were grown by temperature gradient technique (TGT) as shown in Fig. 1. High purity (>99.995%) CaF_2 , PrF_3 , YF_3 and GdF_3 fine powders were used as raw materials, which were mixed with 1.0 wt% PbF_2 (used as oxygen scavenger) and loaded into a graphite crucible [27–29]. The single crystals were grown in the vacuum environment with air pressure less than 3×10^{-3} Pa. The crystal samples were cut and polished for spectral measurements. The XRD tests were carried in Rigaku D/Max 2550 v X-ray diffractometer. Absorption spectra were recorded with a jasco V-570 spectrophotometer. Emission spectra and fluorescence decay curves of the crystals were carried out by a FLS980 time-resolved fluorescence spectrometer (Edinburgh Company, England). The xenon lamp was used as the exciting source. The visible emission was measured by a PMT photodetector.



Fig. 1. Picture of the 0.6at.%Pr: $\text{Ca}_{0.94}\text{Gd}_{0.06}\text{F}_{2.06}$ crystal sample as grown.

3. Results and discussion

The X-ray diffraction tests were carried out at room temperature. The scan range was 10° – 70° with the scanning step of 0.02° .

The X-ray diffraction measurement for the R ions doped Pr: CaF_2 crystals were done at room temperature, as shown in Fig. 2. The observed X-ray peaks for the prepared crystals are matched with the standard JCPDS card (No # 35-0816). The cell remains a cubic fluoride structure after the co-doping process.

The absorption spectra of Pr: $\text{Ca}_{1-x}\text{Y}_x\text{F}_{2+x}$ and Pr: $\text{Ca}_{1-x}\text{Gd}_x\text{F}_{2+x}$ ($x = 0.006, 0.012, 0.03, 0.06$) crystals were measured from 400 to 700 nm at room temperature. The absorption cross-sections are calculated and shown in Fig. 3(a) and (b). The absorption spectra of all the crystals have similar shapes, with four absorption bands in the visible region, which center at 443 nm ($^3\text{H}_4 \rightarrow ^3\text{P}_2$), 468 nm ($^3\text{H}_4 \rightarrow ^3\text{P}_{1+16}$), 482 nm ($^3\text{H}_4 \rightarrow ^3\text{P}_0$) and 592 nm ($^3\text{H}_4 \rightarrow ^1\text{D}_2$). The strongest absorption peak centers at 443 nm matches the emission wavelength of the InGaN laser diode.

Fig. 4(a) and (b) illustrate the emission spectra of the Pr: $\text{Ca}_{1-x}\text{Y}_x\text{F}_{2+x}$ and Pr: $\text{Ca}_{1-x}\text{Gd}_x\text{F}_{2+x}$ ($x = 0.006, 0.012, 0.03, 0.06$) crystals at room temperature. The measurements were conducted under the same conditions to ensure the accuracy and comparability of the emission intensity. All the emission spectra consist of seven bands with peaks at 484 nm ($^3\text{P}_0 \rightarrow ^3\text{H}_4$), 536 nm ($^3\text{P}_0 \rightarrow ^3\text{H}_5$), 598 nm ($^1\text{D}_2 \rightarrow ^3\text{H}_4$), 615 nm ($^3\text{P}_0 \rightarrow ^3\text{H}_6$), 642 nm ($^3\text{P}_0 \rightarrow ^3\text{F}_2$), 694 nm ($^3\text{P}_0 \rightarrow ^3\text{F}_3$) and 727 nm ($^3\text{P}_0 \rightarrow ^3\text{F}_4$), respectively.

Obviously, increasing the proportions of Y^{3+} and Gd^{3+} ions could both enhance the visible emission intensity significantly, especially for the blue (482 nm), orange (598 nm) and red (642 nm) emissions. However, the behaviors of the three emission bands were very different with the different regulators of Y^{3+} or Gd^{3+} , as well as with their doping proportions. The blue ($^3\text{P}_0 \rightarrow ^3\text{H}_4$) and red ($^3\text{P}_0 \rightarrow ^3\text{F}_2$) transitions centered at 496 nm and 656 nm, respectively, shifted to 484 nm and 642 nm after the co-doping process, as shown in Fig. 5. The diversity of composition and structure of the luminescence centers are likely to contribute to the results.

The emission intensity at the above-mentioned eight wavelengths are shown in Fig. 6(a) and (b) with doping proportions of Y^{3+} and Gd^{3+} , respectively. From Fig. 6(a), one can see the behavior of the blue emission at 482 nm is unique, which increases more markedly than others with the proportion of Y^{3+} ions. For the 0.6at.%Pr: CaF_2 crystal, the intensity of red emission was stronger than the blue one, while the phenomenon was inverted and the latter became to be the strongest one among all the visible emission

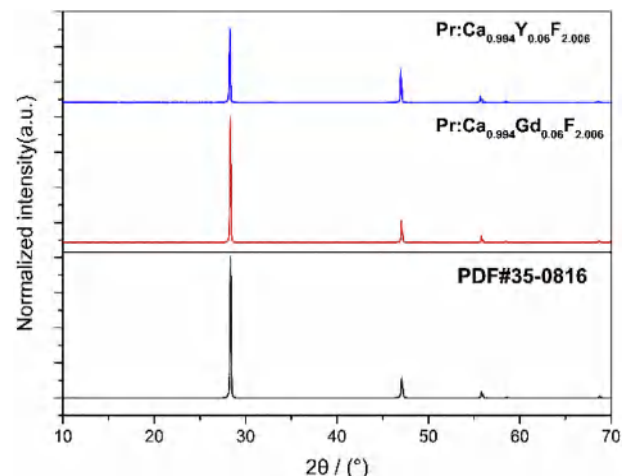


Fig. 2. XRD profiles of Pr: $\text{Ca}_{1-x}\text{R}_x\text{F}_{2+x}$ ($x = 0.006$; R = Y, Gd) crystals.

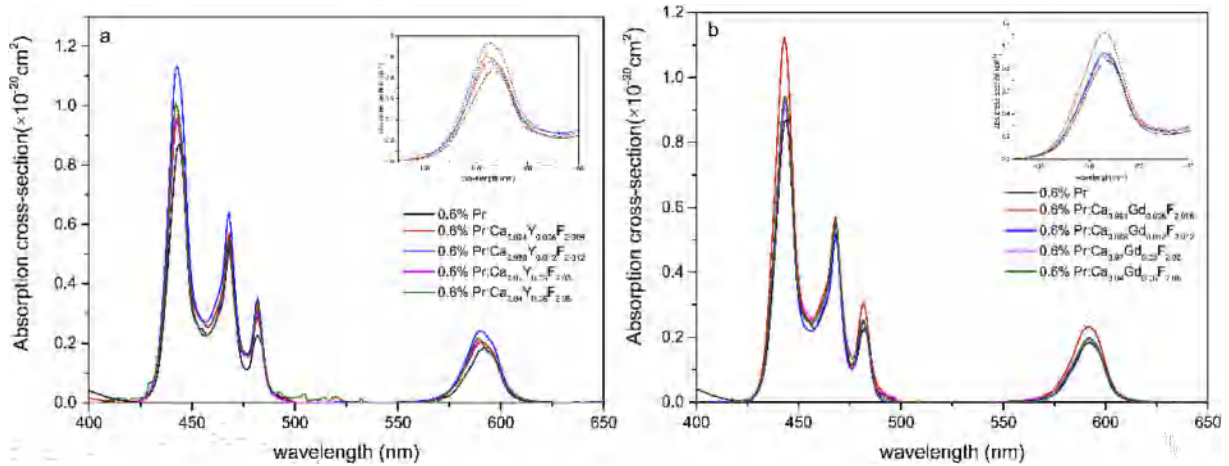


Fig. 3. Absorption cross-section of Pr:Ca_{1-x}Y_xF_{2+x} crystals(a) and Pr:Ca_{1-x}Gd_xF_{2+x} crystals(b); inset: detailed spectrum in the range of 425–460 nm.

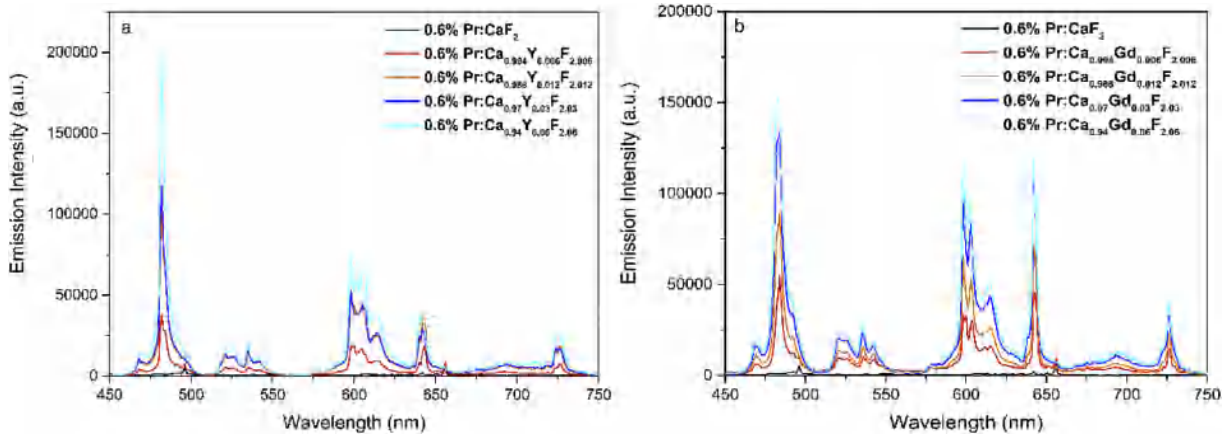


Fig. 4. Room temperature emission intensity of Pr:Ca_{1-x}Y_xF_{2+x} (a) and Pr:Ca_{1-x}Gd_xF_{2+x} crystals(b).

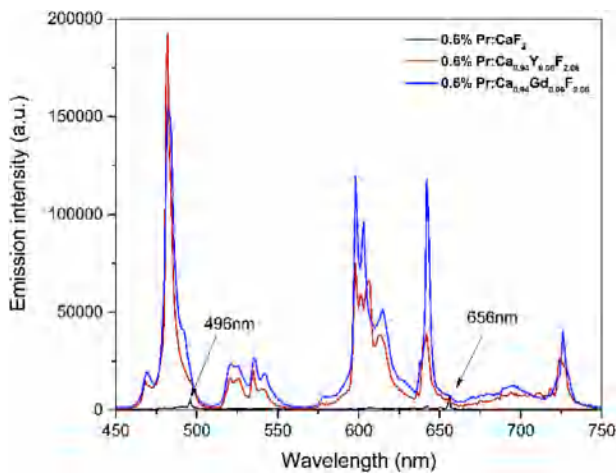


Fig. 5. Room temperature emission intensity of 0.6% Pr:CaF₂, 0.6% Pr:Ca_{0.94}Y_{0.06}F_{2.06} and 0.6%Pr:Ca_{0.94}Gd_{0.06}F_{2.06} crystals.

bands when the concentration of Y³⁺ ions was 0.6at.%. When the value of x increased to 0.06, the intensity of the blue emission was increased to be 35.5times of the red. On the other hand, with the increase of Y³⁺ concentration, the relative fluorescence ratio of

the orange at 598 nm to red at 642 nm (hereafter defined as H₁) and the orange to the blue (defined as H₂) increased from 0.15 to 1.9, 0.09 to 0.39, respectively, as listed in Table 1. Additionally, the value of H₃ (fluorescence ratio of the red at 642nm to blue at 482nm) decreased from 0.44 to 0.20. So, 0.6 at% Pr:Ca_{1-x}Y_xF_{2+x} crystals are promising for blue and orange laser operating.

As for the Pr:Ca_{1-x}Gd_xF_{2+x} crystals. The value of H₁, H₂ and H₃ increased from 0.15 to 1.02, 0.09 to 0.81 and 0.44 to 0.79, respectively, with the increase of Gd³⁺ concentration. As can be seen, Gd³⁺ ions have a more outstanding influence on the red emission at 642nm of the Pr:Ca_{1-x}Gd_xF_{2+x} crystals compared to the crystals co-doped with Y³⁺ ions. When the concentration of Gd³⁺ ions increased to 6.0at.%, the intensity of the red emission was increased to be 16.4 times of the 0.6at.%Pr:CaF₂ crystal. Thus it can be seen that red laser output could be expected from the Pr:Ca_{1-x}Gd_xF_{2+x} crystals.

The enhancement of the emission intensity for the fluorescence bands could be explained by the function of the regulating ions (Y³⁺ or Gd³⁺ ions), which could be used as buffer ions. The co-doping ions enhanced the emission efficiency as compared with the singly doped one. Besides, with the increase of R³⁺ concentration, [Pr³⁺-R³⁺] clusters turned to be more massive and complicated, which aggravated the local lattice structure distortion and led to a further broken of the 4f-4f parity-forbidden transition. Thus the probability of the radiative transition increased, which

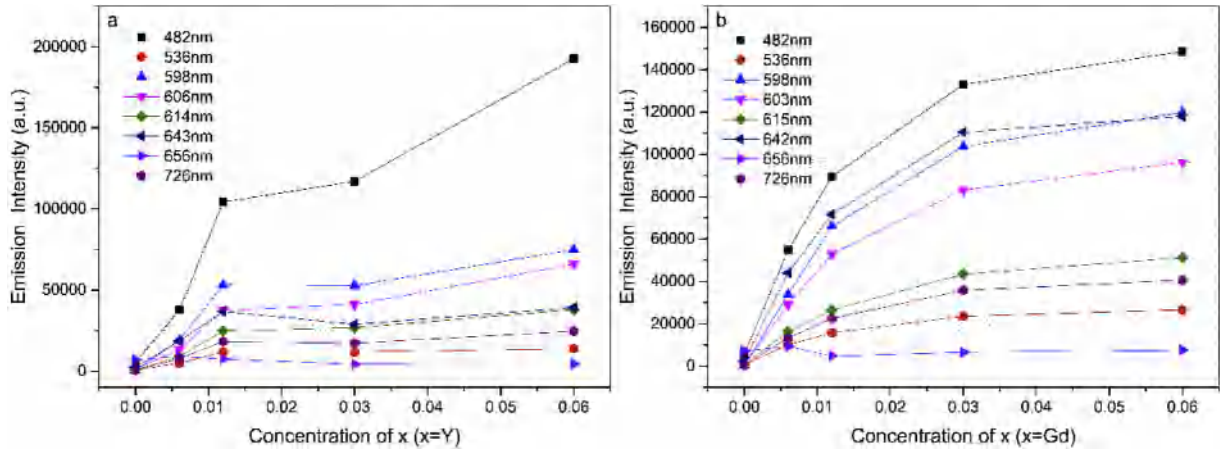


Fig. 6. Emission intensity of the eight visible emission bands for the Pr:Ca_{1-x}Y_xF_{2+x} (a) and Pr:Ca_{1-x}Gd_xF_{2+x} crystals(b) (x = 0.006,0.012,0.03,0.06).

Table 1
Relative emission intensity ratio of the Pr:Ca_{1-x}R_xF_{2+x} crystals.

Concentration of R ³⁺ ions (x)		0	0.006	0.012	0.03	0.06
H ₁ (O/R)	R = Y	0.15	1.02	1.5	1.8	1.9
	R = Gd		0.8	0.91	0.94	1.02
H ₂ (O/B)	R = Y	0.09	0.51	0.51	0.45	0.39
	R = Gd		0.62	0.74	0.78	0.81
H ₃ (R/B)	R = Y	0.44	0.49	0.35	0.25	0.20
	R = Gd		0.80	0.80	0.83	0.79

caused a more intensive fluorescence. However, the influence of the co-doping R³⁺ ions on the emission characteristics could bevarious. Although The blue (482nm) and red (642nm) emissions both emit from the ³P₀ energy level, the change regulation of fluorescence intensity ratio with the increasing of Y³⁺ or Gd³⁺ ions could be different, which might be explained by the different microstructures that the [Pr³⁺-Y³⁺] clusters and [Pr³⁺-Gd³⁺] clusters owned.

The fluorescence decay curves at 727 nm (corresponding to Pr³⁺:³P₀energy level) of these two series of crystals were recorded at room temperature. As shown in Fig. 7(a) and (b), the decay curves exhibited multiple-exponential behavior. The increase of R³⁺ concentration as a function of the fluorescence lifetimes are shown in Fig. 7(a) and (b). When the concentration of R³⁺ was 0.6at.%, the long lifetimes of Y³⁺ co-doped and Gd³⁺ crystals decreased sharply from 121 μs to 57 μs and 49 μs, respectively.

The long lifetime increased slowly from to 61 μs with the increase of Y³⁺ concentration. While it decreased slowly from 23 μs to 48 μs when the co-doping ion is Gd³⁺. The short lifetimes of the two series of crystals increased slowly from 23 μs to 41 μs(Pr:Ca_{1-x}Y_xF_{2+x} crstals) and 31 μs(Pr:Ca_{1-x}Gd_xF_{2+x} crystals), respectively, with the increase of R³⁺ concentration. The gap between long lifetime and short lifetimes of the Pr:Ca_{1-x}R_xF_{2+x} crstals reduce significantly compared with the Pr:CaF₂ crystal, which indicates that the discrepancy of luminescence center structures in the Pr:Ca_{1-x}Gd_xF_{2+x} crstals are reduced (see Fig. 8).

We have then calculated the average lifetime of the crystals by using the formula as follows:

$$\tau_{\text{avg}} = \frac{A_s \tau_s^2 + A_l \tau_l^2}{A_s \tau_s + A_l \tau_l} \quad (1)$$

where τ_{avg} is the mean lifetime. A_s and A_l are the preexponential factors, which are defined by the nature of the reaction and unrelated to the concentration of the doped ions. τ_s and τ_l and the short lifetime and the long life time obtained from the mentioned calculation results.

The lifetime for the 0.6%Pr:Ca_xY_{1-x}F_{x+2} crystals increased from 25μs to 47μs when the value of x increased to 0.06. While it increased from 25 μs to 44 μs when the co-doping ion is Gd³⁺. The non-radiative decay channels of the energy transfers among the Pr³⁺ ions have been reduced after the co-doping process [26].

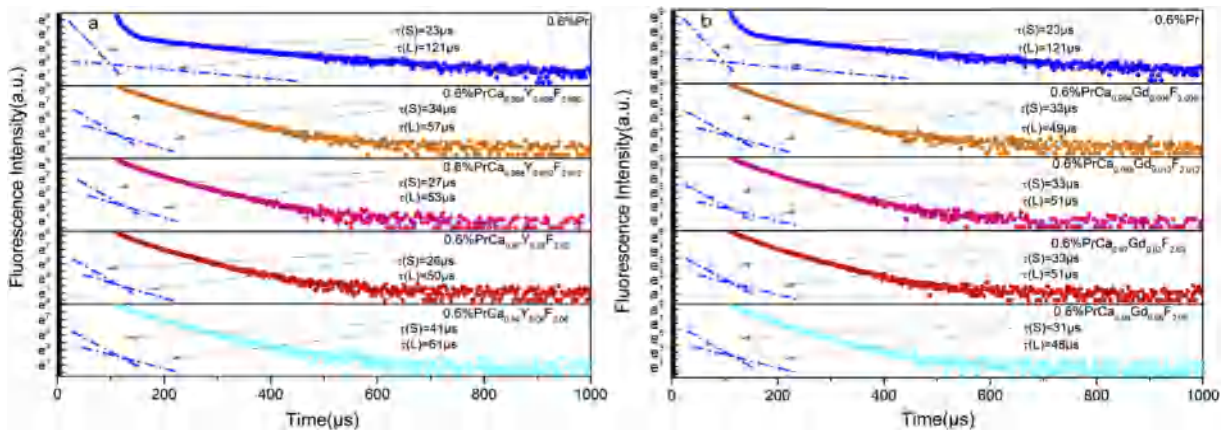


Fig. 7. Decay curves of Pr:Ca_{1-x}Y_xF_{2+x} (a) and Pr:Ca_{1-x}Gd_xF_{2+x} crystals(b) (x = 0.006,0.012,0.03,0.06) at room temperature.

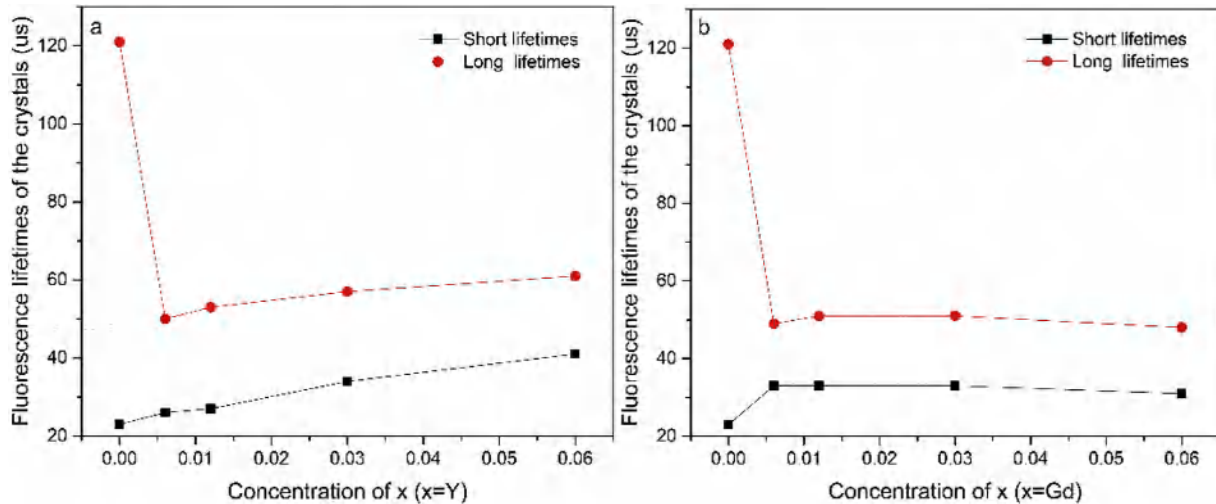


Fig. 8. Fluorescence times of the $\text{Pr:Ca}_{1-x}\text{Y}_x\text{F}_{2+x}$ (a) and $\text{Pr:Ca}_{1-x}\text{Gd}_x\text{F}_{2+x}$ crystals(b) ($x = 0.006, 0.012, 0.03, 0.06$).

The internal Quantum efficiency (QE), defined as the ratio of the number of emitted photons to the number of photons absorbed, were measured using the absolute techniques [30] with a barium sulfate-coated integrating sphere (Edinburgh Instruments, EI) as the sample chamber at room temperature. The entry and output gates of the sphere located in 90-degree geometry from each other in the plane of the fluorimeter. Both emissions of the reference plane and crystal samples were collected in the region of 430 nm–750 nm with the Xenon lamp excitation at 443 nm, and the data was also corrected for the spectral response of the integrating sphere. Then the results were calculated by the internal system of the spectrometer (see Fig. 9).

As can be seen from Fig. 10, the quantum efficiency of the two series of crystals increased rapidly and tend to be 100% with the increment of R^{3+} concentration. As for $\text{Pr:Ca}_{1-x}\text{Y}_x\text{F}_{2+x}$ crystals, the quantum efficiency tended to be saturated at a relative low concentration of 3.0at.% Y^{3+} . However, for the $\text{Pr:Ca}_{1-x}\text{Gd}_x\text{F}_{2+x}$ crystals, the quantum efficiency continuously increased with the increment of Gd^{3+} concentration. It is worth mentioning that Pr:CaF_2 crystal has an extremely low quantum efficiency that could not be

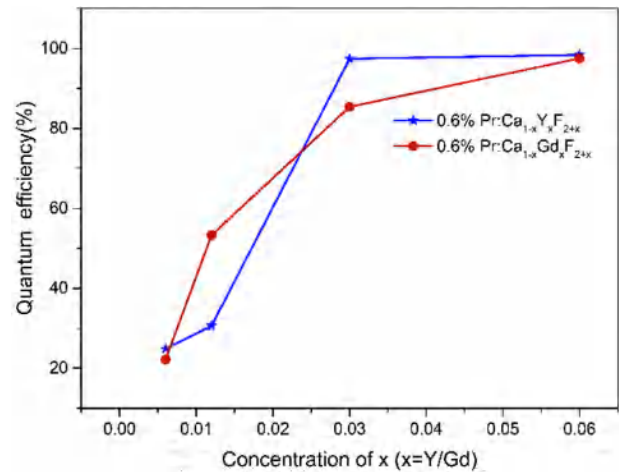


Fig. 10. Quantum efficiency of the $\text{Pr:Ca}_{1-x}\text{Y}_x\text{F}_{2+x}$ and $\text{Pr:Ca}_{1-x}\text{Gd}_x\text{F}_{2+x}$ crystals ($x = 0.006, 0.012, 0.03, 0.06$).

determined under the current experiment conditions, mainly because of the quenching effect. The quantum efficiencies of the co-doped crystals in agreement with the fluorescence lifetimes, which proved that the non-luminescent Pr^{3+} ions clusters are reduced by co-doping Pr:CaF_2 crystals with Y^{3+} or Gd^{3+} ions.

4. Conclusions

The experimental results show that co-doping Pr:CaF_2 crystals with Y^{3+} ions and Gd^{3+} ions could significantly improve the spectral properties of the crystals in the visible wavelength region. The emission intensity of all visible emission bands increased with the proportion of Y^{3+} and Gd^{3+} in $\text{Pr:Ca}_{1-x}\text{R}_x\text{F}_{2+x}$ crystals, but not of the same trend. For the $\text{Pr:Ca}_{1-x}\text{Y}_x\text{F}_{2+x}$ crystals, the blue emission band at 482 nm increases more markedly than others and becomes the strongest band. When x was increased to 0.06, the blue intensity increased to be 35.5 times of the 0.6at.% Pr:CaF_2 crystal. The second one is the orange emission band at 598 nm with 156 times. As for the $\text{Pr:Ca}_{1-x}\text{Gd}_x\text{F}_{2+x}$ crystals, the Gd^{3+} ions have the most outstanding influence on the red fluorescence band at 642nm. The lifetime for 0.6% $\text{Pr:Ca}_x\text{Y}_{1-x}\text{F}_{x+2}$ and 0.6% $\text{Pr:Ca}_x\text{Gd}_{1-x}\text{F}_{x+2}$ crystals increased from 25 μs to 47 μs and 44 μs , respectively, when the value

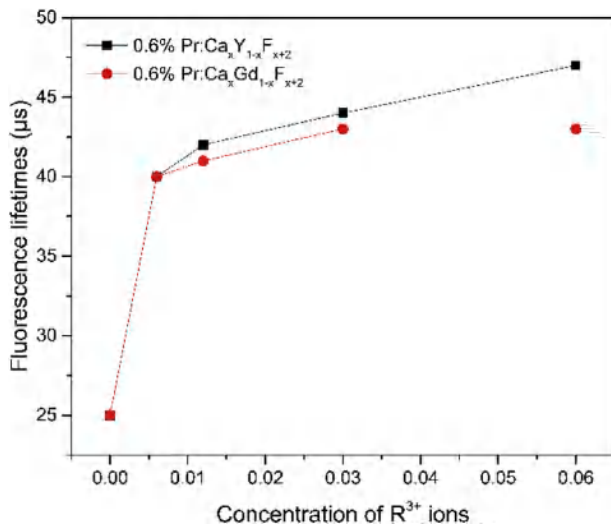


Fig. 9. Mean fluorescence times of the $\text{Pr:Ca}_{1-x}\text{Y}_x\text{F}_{2+x}$ (a) and $\text{Pr:Ca}_{1-x}\text{Gd}_x\text{F}_{2+x}$ crystals(b).

of x increased to 0.06. The internal quantum efficiencies of the crystals increased with the increment of the proportion of Y^{3+} or Gd^{3+} ions, and finally tend to be 100%. So, Pr-doped $Ca_{1-x}Y_xF_{2+x}$ and $Ca_{1-x}Gd_xF_{2+x}$ crystals would be very promising for visible laser applications at blue, orange, and red bands, respectively.

Funding

The author acknowledge support from the National Key Research and Development Program of China (No.2016YFB0701002), and the National Natural Science Foundation of China (Nos.61635012, 61475177, 61422511).

References

- [1] L. Esterowitz, R. Allen, M. Krueger, F. Bartoli, L.S. Goldberg, H.P. Jenssen, A. Linz, V.O. Nicolai, *J. Appl. Phys.* 48 (1977) 650.
- [2] X. Lu, Z. You, J. Li, Z. Zhu, G. Jia, B. Wu, C. Tu, *Appl. Phys. B* 85 (2006) 585–589.
- [3] C. Zaldo, M. Rico, C. Cascales, M.C. Pujol, J. Massons, M. Aguiló, F. Díaz, P. Porcher, *J. Phys. Condens. Matter* 12 (2000) 8531.
- [4] G. Jia, H. Wang, X. Lu, Z. You, J. Li, Z. Zhu, C. Tu, *Appl. Phys. B* 90 (2008) 497–502.
- [5] W.J. Guo, Y.F. Lin, X.H. Gong, Y.J. Chen, Z.D. Luo, Y.D. Huang, *Appl. Phys.* 104 (2008), 053105.
- [6] D. Serrano, A. Braud, J. Doualan, P. Camy, R. Moncorgé, *Opt. Soc. Am. B* 29 (2012) 1854.
- [7] F. Xiong, X. Lin, Z. Luo, G. Tan, E. Ma, Y. Huang, *J. Appl. Phys.* 99 (2006) 064905–064908.
- [8] F. Reichert, F. Moglia, D.T. Marzahl, P. Metz, M. Fechner, N. Hansen, G. Huber, *Optic Express* 20 (2012) 20387–20395.
- [9] M. Fibrich, H. Jelinkova, J. Sulc, K. Nejezchleb, V. Skoda, *Laser Phys. Lett.* 8 (2011) 559–568.
- [10] L.D. Merkle, B. Zandi, R. Moncorgé, Y. Guyot, H.R. Verdun, B. Intosh, *Appl. Phys.* 79 (1996) 1849–1856.
- [11] P. Metz, F. Reichert, F. Mogila, S. Müller, D. Marzahl, C. Kränkel, G. Huber, *Opt. Lett.* 39 (2014) 3193.
- [12] B. Xu, Z. Liu, H. Xu, Z. Cai, C. Zeng, S. Huang, Y. Yan, F. Wang, P. Camy, J.L. Doualan, A. Braud, R. Moncorgé, *Opt. Commun.* 96 (2013) 305.
- [13] S.Y. Luo, X.G. Yan, Q. Cui, B. Xu, H.Y. Xu, Z.P. Cai, *Opt. Commun.* 380 (2016) 357–360.
- [14] A. Richer, E. Heumann, E. Osic, G. Huber, W. Seelert, A. Dening, *Opt. Lett.* 29 (2004) 2638–2640.
- [15] P.W. Metz, S. Müller, F. Reichert, D.T. Marzahl, F. Moglia, C. Kränkel, G. Huber, *Opt. Express* 21 (2013) 31274–31281.
- [16] D. Pabœuf, O. Mhibik, F. Bretenaker, P. Goldner, D. Parisi, M. Tonelli, *Opt. Lett.* 36 (2011) 280–282.
- [17] F. Cornacchia, A. Richter, E. Heumann, G. Huber, D. Parisi, M. Tonelli, *Opt. Express* 15 (2007) 992–1002.
- [18] L. Dressler, R. Rauch, R. Reimann, *Cryst. Res. Technol.* 23 (1992) 413–420.
- [19] P. Camy, J.L. Doualan, A. Benayad, M. Von Edlinger, V. Menard, R. Moncorgé, *Appl. Phys. B* 89 (2007) 539.
- [20] P.A. Popov, P.P. Fedorov, S.V. Kuznetsov, V.A. Konyushkin, V.V. Osiko, T.T. Basiev, *Dokl. Phys.* 53 (2008) 413–415.
- [21] P.A. Popov, P.P. Fedorov, V.A. Konyushkin, *Crystallogr. Rep.* 60 (2015) 744–748.
- [22] M. Siebold, M. Hornung, R. Boedefeld, S. Podleska, S. Klingebiel, C. Wandt, F. Krausz, S. Karsch, R. Uecker, A. Jochmann, J. Hein, M. Christoph Kaluza, *Opt. Lett.* 33 (2008) 2770–2772.
- [23] M. Hornung, H. Liebetrau, S. Keppler, A. Kessler, M. Hellwing, F. Schorch, G.A. Becker, M. Reuter, J. Polz, J. Körner, J. Hein, M.C. Kaluza, *Opt. Lett.* 41 (2016) 5413–5416.
- [24] Z.P. Qin, G.Q. Xie, J. Ma, W.Y. Ge, P. Yuan, L.J. Qian, L.B. Su, D.P. Jiang, F.K. Ma, Q. Zhang, Y.X. Cao, J. Xu, *Opt. Lett.* 39 (2014) 1737–1739.
- [25] B.M. Tissue, J.C. Wright, *Phys. Rev. B* 18 (1987) 9781–9789.
- [26] J.L. Doualan, P. Camy, R. Moncorgé, E. Daran, M. Couchaud, B. Ferrand, *J. Fluorine Chem.* 128 (2007) 459–464.
- [27] B.P. Sobolev, *The Rare Earth Trifluorides, Part 1: the High Temperature Chemistry of the Rare Earth Trifluorides*, Institute of Crystallography, Moscow, 2000.
- [28] B.P. Sobolev, *The Rare Earth Trifluorides, Part 2: Introduction to Materials Science of Multicomponent Metal Fluoride Crystals*, Institute of Crystallography, Moscow, 2000.
- [29] P.P. Fedorov, V.V. Osiko, *Crystal growth of fluorides*, in: P. Capper (Ed.), *Bulk Crystal Growth of Electronic, Optical and Optoelectronic Materials*, John Wiley & Son. Ltd., Moscow, 2005, pp. 339–356.
- [30] C. Würth, M. Grabolle, J. Pauli, M. Spieles, U. Resch-Genger, *Nat. Protoc. Anal. Chem.* 8 (2011) 1535.